AGU PUBLICATIONS

Geophysical Research Letters

RESEARCH LETTER
10.1002/2014GL062269

Key Points:
- The phase transition of PDV is dominated by the natural internal variability
- External forcing dominates the trend of PDV index and modulates its magnitude
- The combined effects of GHGs and aerosols favor the positive phase of PDV

Supporting Information:
- Readme
- Tables S1 and S2 and Figures S1–S8

Correspondence to:
T. Zhou,
zhoutj@lasg.iap.ac.cn

Citation:
Dong, L., T. Zhou, and X. Chen (2014), Changes of Pacific decadal variability in the twentieth century driven by internal variability, greenhouse gases, and aerosols, *Geophys. Res. Lett.*, *41*, doi:10.1002/2014GL062269.

Changes of Pacific decadal variability in the twentieth century driven by internal variability, greenhouse gases, and aerosols

Lu Dong[1,2], Tianjun Zhou[1,3], and Xiaolong Chen[1,2]

[1]State Key Laboratory of Numerical Modeling for Atmospheric Sciences and Geophysical Fluid Dynamics, Institute of Atmospheric Physics, Chinese Academy of Sciences, Beijing, China, [2]College of Earth Science, University of Chinese Academy of Sciences, Beijing, China, [3]Climate Change Research Center, Chinese Academy of Sciences, Beijing, China

Abstract This paper explores the contributions of internal variability, greenhouse gases (GHGs), and anthropogenic aerosols (AAs) in driving the magnitude and evolution of Pacific Decadal Variability (PDV) during the twentieth century by analyzing 129 Coupled Model Intercomparison Project Phase 5 model realizations. Evidence shows that PDV phase transition is dominated by internal variability, but it is also significantly affected by external forcing agents such as GHGs and aerosols. The combined effects of GHGs and AAs favor the positive phase of PDV with stronger ocean warming in the tropics than the extratropical Pacific. The GHG forcing induces the increased surface downward longwave radiation, especially over the tropical Pacific, and results in stronger warming in that area. The AA forcing results in a stronger cooling in the North Pacific region, due to the reduced surface downward shortwave radiation via cloud-aerosol interaction: this offsets the substantial warming caused by GHG forcing.

1. Introduction

Pacific Decadal Variability (PDV) is one of the most important climate phenomena and is a key component in the predictability of both regional and global climate change. It is generally called Interdecadal Pacific Oscillation (IPO) for the basin-wide pattern [*Power et al.*, 1999], or Pacific Decadal Oscillation (PDO) for the North Pacific pattern [*Mantua et al.*, 1997]. The time series of PDO and IPO are highly correlated [*IPCC*: *Climate Change*, 2013]. The positive phase of PDV is characterized by positive sea surface temperature (SST) anomalies in the tropical Pacific and along the west coasts of North and South America, with negative SST anomalies in the central and western North Pacific. Observations have shown that PDV has shifted phase several times during the twentieth century, most notably in 1976 [*Mantua et al.*, 1997; *Mantua and Hare*, 2002]. Such phase transitions have been associated with long-term fluctuations of Australian rainfall [*Power et al.*, 1999; *Arblaster et al.*, 2002], major changes in the ecosystem of the North Pacific [*Mantua et al.*, 1997], summer precipitation and monsoon over East Asia [*Li et al.*, 2010; *Zhou et al.*, 2009, 2013; *Qian and Zhou*, 2014; *Yu et al.*, 2014], and Alaskan, northeastern Siberian, Manchurian, Korean, and Japanese hydroclimatology [*Mantua and Hare*, 2002; *Deser et al.*, 2004].

The impact of anthropogenic climate change on the modes of internal variability in the climate system is a key issue for climate science. For example, the SST warming pattern in the Indian Ocean modulates the Indian Ocean Dipole via global warming [*Zheng et al.*, 2013; *Cai et al.*, 2014]. PDV can modulate seasonal and interannual climate variability [*Fang et al.*, 2014], such as the El Niño–Southern Oscillation (ENSO) [e.g., *Fedorov and Philander*, 2000; *Yeh et al.*, 2012; *Xiang et al.*, 2013] and the relationship between the ENSO and climate over East Asia and North America [*Barlow et al.*, 2001; *Wang*, 2002; *Yoon and Yeh*, 2010]. *Verdon and Franks* [2006] suggested that El Niño (La Niña) events are more likely to occur during a positive (negative) PDV phase. In a similar way, as decadal-scale variability, PDV may be modulated by longer-scale background changes, such as the centennial trend investigated in this study. Given PDV's major links with global climate change, its change in a warming world, and the possible mechanism are of great importance.

PDV is commonly regarded as an internal mode of climate system and may be influenced by external forcing (mainly including solar variability, volcanic eruptions, greenhouse gases (GHGs), and anthropogenic aerosols (AAs)). External forcing may have contributed to the observed PDV transition in the mid-1970s, through superimposing on internal variability [*Meehl et al.*, 2009]; however, which kind of external forcing dominated the contribution is unclear. Under GHG forcing, PDV does not exhibit significant changes in spatial and

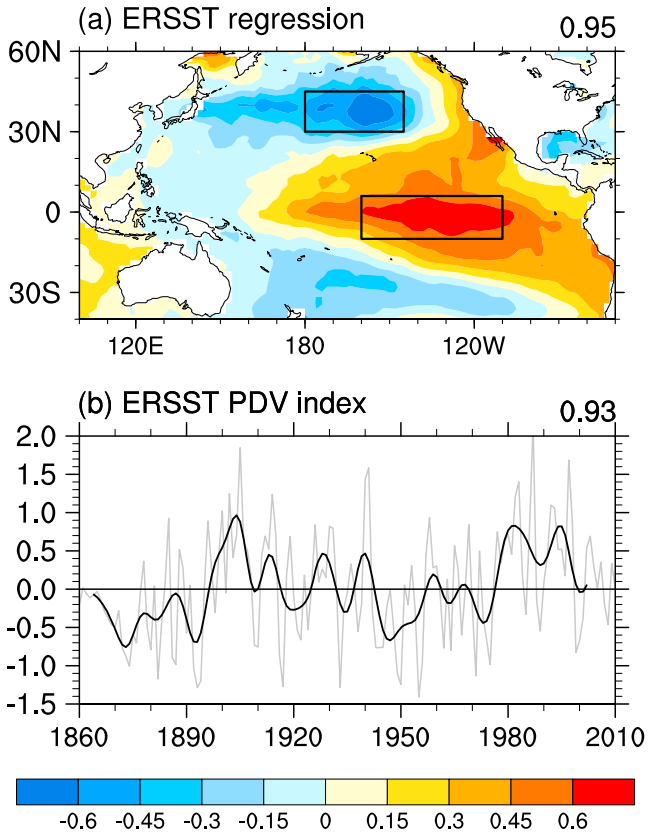

Figure 1. (a) The pattern and (b) the time series of PDV in observation during 1861–2010. PDV index (black line) is defined as the 9 year low-pass-filtered SST anomaly difference between the eastern tropical Pacific (10°S–6°N, 110°W–160°W) and North Pacific (30°N–45°N, 145°W–180°W). The annual mean time series is shown as a grey line. PDV pattern is obtained by regressing SST anomalies onto PDV index. The numbers at the top right denote the correlation coefficient with IPO defined from the EOF method as shown in Figure S1.

temporal characteristics in most Coupled Model Intercomparison Project Phase 3 (CMIP3) models [*Furtado et al.*, 2011] but becomes weaker and more frequent in the Fast Ocean Atmosphere Model [*Fang et al.*, 2014]. External forcing can project onto PDV pattern through changing the tropical-extratropical SST anomaly contrast in the Pacific, and thus has the potential to influence PDV [*Wang et al.*, 2012]. Some models show that GHG forcing leads to a weak and nonsignificant shift toward more occurrences of the negative phase of PDV, early in the 21st century [*Lapp et al.*, 2011]. Some models show that AA acted to modify PDV and forced the trends of PDV in the twentieth century historical simulations [*Allen et al.*, 2014]. However, others stress the importance of the strong tropical volcanic eruptions in regulating PDV in favor of the negative phase [*Wang et al.*, 2012]. Up to now, there has been no consensus on the effects of different external forcings in PDV change.

The purpose of this paper is to explore whether different external forcings affect PDV through changing the tropical-extratropical SST anomaly contrast in the Pacific during the twentieth century.

2. Observations, Model Experiments, and Method

The National Oceanic and Atmospheric Administration Extended Reconstructed SST version 3 (ERSST V3, $2° \times 2°$) is used in this study [*Smith et al.*, 2008], which is a reconstructed data set, and "analysis" procedures are performed, such as spatial or temporal smoothing or interpolation [*Deser et al.*, 2010]. It is regarded as the "observed" SST data in this study. We select this data set for analysis as it well exhibits the trends in the tropical SST during the twentieth century [*Deser et al.*, 2010].

We analyze a total of 129 realizations from eight Coupled Model Intercomparison Project Phase 5 (CMIP5) models, comprising 45 historical, 28 historical GHG, 30 historical natural (Nat), and 26 historical AA experiments (see Table S1 in the supporting information) [*Taylor et al.*, 2012]. The twentieth century historical climate simulations (called *all forcing*) are forced by natural agents (solar radiation and volcanic aerosols) and anthropogenic agents (mainly GHGs, AAs, ozone, and land use). The historical GHG, historical Nat, and historical AA simulations are only forced by well-mixed GHGs, natural agents, or AA forcing, respectively, with other forcings fixed at the preindustrial level [*Taylor et al.*, 2012]. The specific external forcing agents used in each model are listed in Table S2. We select these eight models for the following two reasons: First, all the outputs of historical, historical GHG, historical Nat, and historical AA experiments are available; second, both the direct and indirect effects of aerosols are considered. The multimodel ensemble (MME) was calculated as the arithmetic mean of the models, with the same weight for each model.

We define PDV index as the SST anomaly differences between the two key regions, the eastern tropical Pacific (10°S–6°N, 110°W–160°W) and the North Pacific (30°N–45°N, 145°W–180°W). The SST anomaly is calculated by

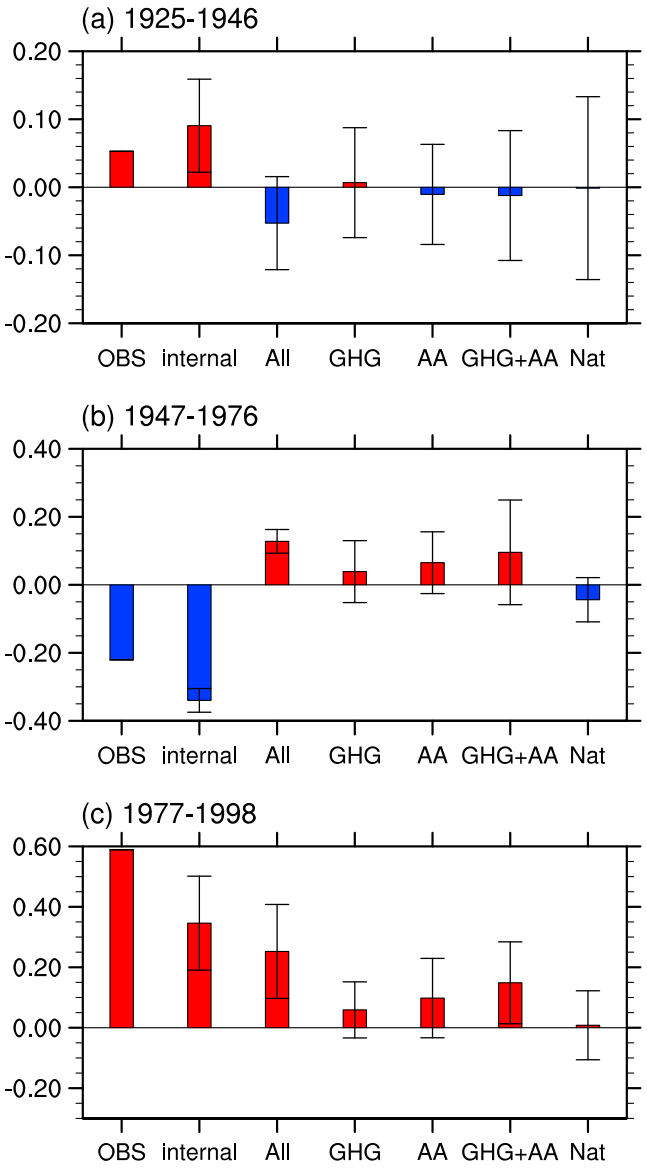

Figure 2. The period mean of PDV index in observation, internal variability (observation minus the MME of all forcing runs), external forcing (the MME of all forcing runs), GHG forcing (the MME of GHG forcing runs), AA forcing (the MME of AA forcing runs), both GHG and AA forcing (the sum of GHG and AA forcing), and natural forcing (the MME of natural forcing runs) during (a) 1925–1946, (b) 1947–1976, and (c) 1977–1998. The error bars denote the standard deviation of intermodel variability. Units: K.

removing the climatological state. In order to focus on the decadal variability, a 9 year low-pass filter is applied onto the SST anomaly. It is more convenient to discuss external forcing effects than the empirical orthogonal function (EOF) definition. As the EOF definition may distribute external forcing signals into different EOF modes, the external forcing effects may be incomplete when only the one PDV mode is analyzed. In addition, the EOF definition with the time-dependent global-averaged SST anomaly removed is not appropriate for the MME of historical simulations, which mainly feature the global-scale changes.

Note that the reduced effective degrees of freedom due to the low-pass filter have been considered when computing the statistical significance based on Monte Carlo test. The process of significance testing is as follows: (1) Generate two random sequences using a normal distribution and apply the 9 year low-pass filter on them; (2) compute the linear trends or the correlation coefficient of the two sequences; (3) Repeat steps 1 and 2 for 5000 times; and (4) sort the trends or correlation coefficients in ascending order. The values for the 95th and 99th percentiles are chosen as the significant correlation values for the 5% and 1% levels, respectively.

All the models are regridded onto a horizontal resolution of 2.8°×2.8°, the lowest resolution among these eight CMIP5 models, and the monthly products are converted to yearly variables. We choose the common period 1861–2005, present for all the data sets, for analysis. Following *Xie et al.* [2013], for a given type simulation, we obtain the multimember average for each model first, in order to reduce the effect of internal variability, and then construct the MME to estimate different forcing effects. However, the heat budget analysis in Figure 5 and Figures S6–S8 is based on the MME of only one member for each model's simulation, and it will not affect the main conclusion as we focus on the long-term trend.

The observed temporal phases of internal modes cannot be reproduced by coupled climate models. The MME of the twentieth century simulations reflects only external forcing variations as internal variability has been averaged out, while the observation contains both external forced components and internal variability. In addition, as the twentieth century simulations are forced with observed atmospheric composition changes reflecting both natural and anthropogenic forcing [*Zhou and Yu*, 2006; *Jha et al.*, 2014], the external forcing of

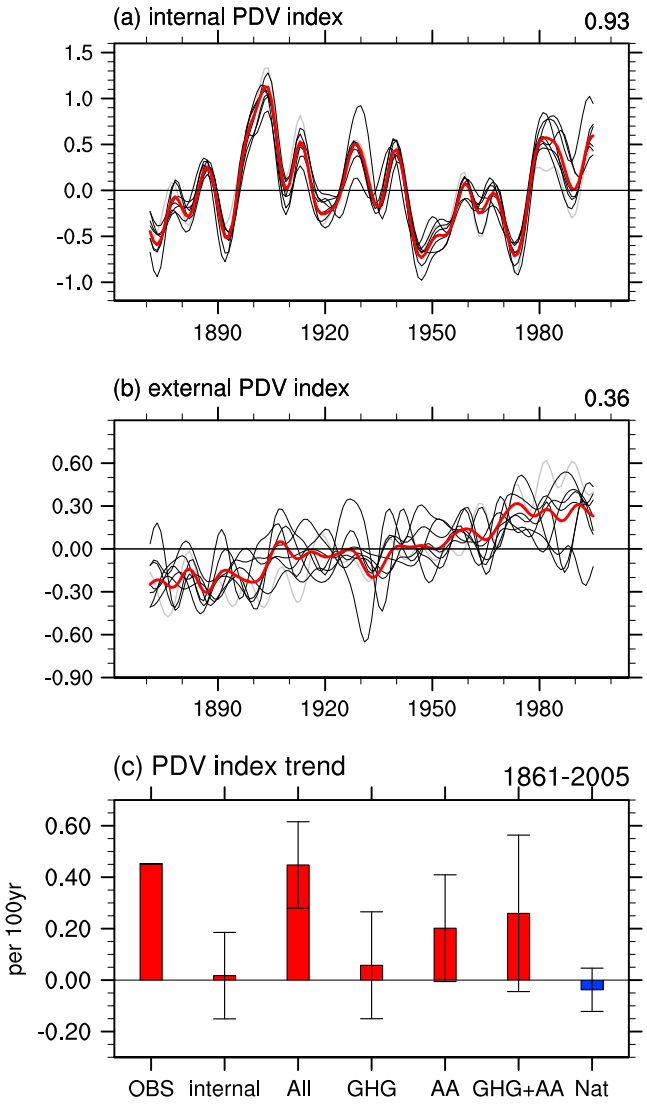

Figure 3. Time series of PDV index (in K) from (a) internal variability and (b) external forcing. The grey lines represent the multimember average for each model, and the red line represents the MME. The number at the top right denotes the correlation coefficient between MME and the observation. (c) The linear trends of PDV index during 1861–2005 in observation, internal variability, external forcing, GHG forcing, AA forcing, both GHG and AA forcing, and natural forcing. The error bars denote the standard deviation of intermodel variability. Units: K (100 years)$^{-1}$.

MME is the same as that in observation and can be removed from observation. Therefore, the difference between the observation and the MME of the twentieth century simulations would be internal variability.

3. Results

The pattern and time series of PDV in the observation are shown in Figure 1. PDV pattern and index are well correlated with IPO defined by the EOF method [*Mantua et al.*, 1997; *Meehl et al.*, 2009; *Bonfils and Benjamin*, 2011]. The correlation coefficient is 0.95 (0.93) for the pattern (index), statistically significant at the 1% level (Figures 1 and S1). The negative to positive transitions occurred during 1896, 1925, and 1976; and those from positive to negative during 1946 and 1998 (Figure 1b). The phase transition time is generally consistent with previous studies [e.g., *Mantua and Hare*, 2002; *Chen et al.*, 2008; *Meehl et al.*, 2009; *Yu et al.*, 2014]. There is a positive trend of 0.45 K (100 years)$^{-1}$ in PDV index, statistically significant at the 5% level (Figure 1b), which also exists in IPO index defined from the EOF method (Figure S1b). Therefore, PDV index used in our study represents well the characteristics of IPO.

Different forcing runs from MME are analyzed to investigate their contributions to the magnitude of PDV during the three main phases of the twentieth century (Figure 2). They are the positive phases during 1925–1946 and 1977–1998, and a negative phase during 1947–1976. Internal variability dominates PDV magnitude in all the three phases, while external forcing has different contributions in the three periods. During 1925–1946, external forcing has a negative contribution to the positive phase of the observation, while it has a positive phase contribution during the late half of the twentieth century, which weakens the 1947–1976 negative phase and enhances the 1977–1998 positive phase. The effect of external forcing is mainly attributed to the combined effects of GHG and AA forcings. Natural forcing effect is negligible. However, uncertainties among these eight models should be noted, and the differences between external forcing and the sum of GHG, AA, and natural forcings may be attributed to the ozone and land use forcings, or the nonlinear parts among different forcings.

Since the anomaly is calculated with respect to the climatology for the whole period, the negative (positive) anomaly of external forcing during the early (late) half of twentieth century implies a pronounced upward trend for PDV index of external forcing. To test this hypothesis, we compare PDV index under internal variability and external forcing in Figure 3. Under internal variability, it is well correlated with that in observation, having a

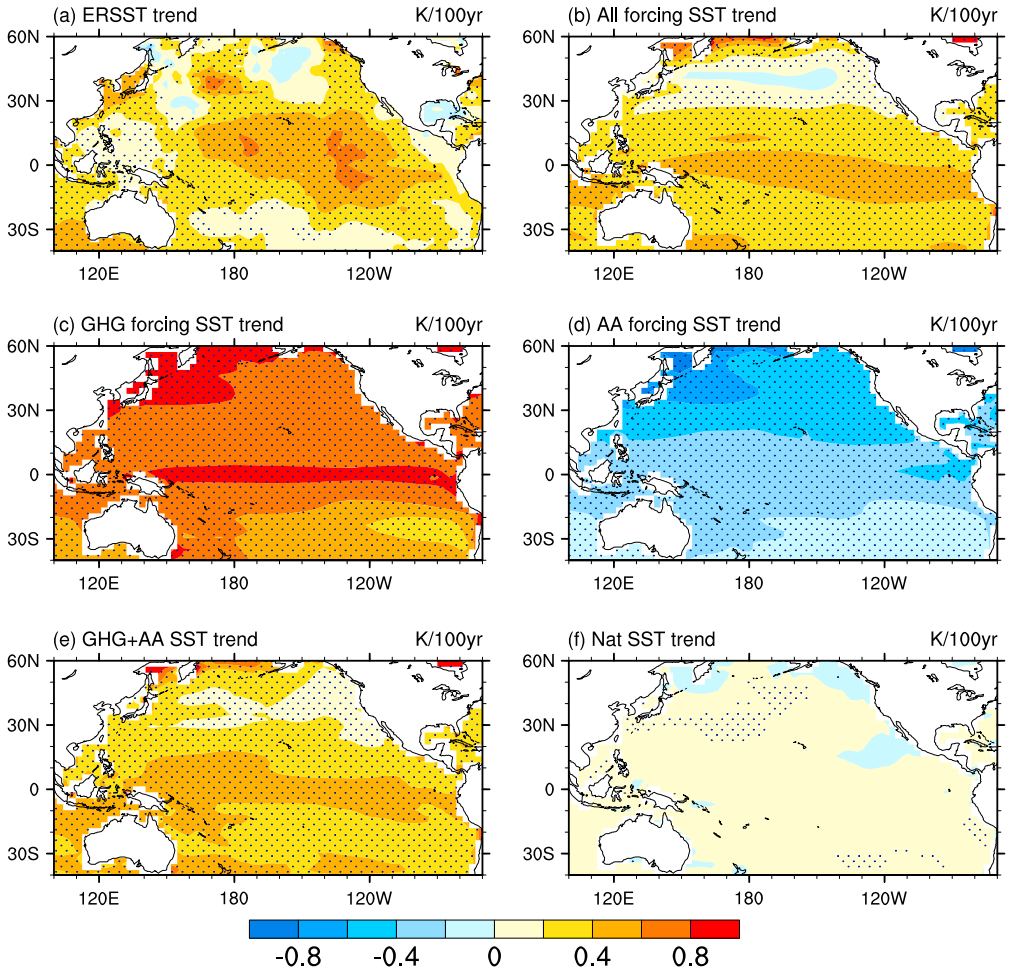

Figure 4. The trend patterns of SST under (a) observation, (b) external forcing, (c) GHG forcing, (d) AA forcing, (e) both GHG and AA forcing, and (f) natural forcing. The dotted areas are statistically significant at the 5% level by Student's *t* test. Units: K (100 years)$^{-1}$.

correlation coefficient of 0.93 based on MME, statistically significant at the 1% level (Figure 3a). The phase transitions around 1896, 1925, 1946, and 1976 still exist, indicating the dominant role of internal variability in the phase transition of PDV during the twentieth century. Under external forcing, PDV index shows a significant positive trend, suggesting that external forcing favors a shift toward the positive phase of PDV (Figure 3b). For the period of 1861–2005, the trend of external forcing is the same as that of the observation (0.45 K (100 years)$^{-1}$), indicating that the positive trend in the observation is totally induced by external forcing and internal variability contributes no apparent trend for this period (Figure 3c). The effect of AA (0.2 K (100 years)$^{-1}$) dominates the positive trend, whereas the GHG forcing (0.06 K (100 years)$^{-1}$) contributes only a small part (Figure 3c). The combined effects of GHG and AA account for about 57.8% of PDV trend in external forcing.

Changing the time period to 1920–2005 or 1950–2005 (Figure S2), PDV index in the observation still shows a positive trend. External forcing also contributes a positive trend, as well as GHGs and AAs, which is robust regardless of the different time periods. However, the contributions of internal variability are different, with the smaller trend for the longer time span. As we mainly focus on the contributions of external forcing in the rest of the paper, and the longer time period is more suited to discuss internal variability, we just analyze the time period of 1861–2005 in the following section.

To understand why external forcing favors the positive phase of PDV, the SST trend patterns under different forcings are compared (Figure 4). In the observation, the eastern tropical Pacific shows a stronger

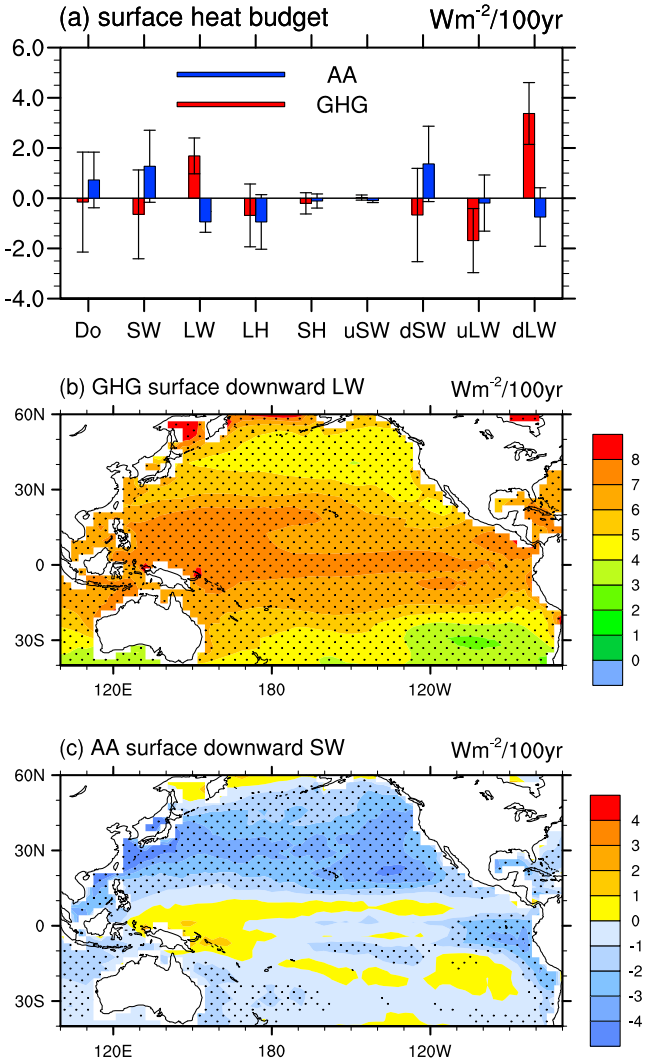

Figure 5. (a) The linear trend differences between the eastern tropical Pacific (10°S–6°N, 110°W–160°W) and the North Pacific region (30°N–45°N, 145°W–180°W) for the ocean heat transport effect (Do), surface net shortwave radiation (SW), surface net longwave radiation (LW), latent heat flux (LH), sensible heat flux (SH), surface upward shortwave radiation (uSW), surface downward shortwave radiation (dSW), surface upward longwave radiation (uLW), and surface downward longwave radiation (dLW), during 1861–2005 under GHG forcing (red bars) and AA forcing (blue bars). The error bars denote the standard deviation of intermodel variability. (b) The trend patterns of surface downward longwave radiation under GHG forcing. (c) The trend patterns of surface downward shortwave radiation under AA forcing. The dotted areas are statistically significant at the 5% level by Student's *t* test. Units: W m^{-2} (100 years)$^{-1}$.

warming than the North Pacific, inducing a positive PDV-like pattern (Figure 4a). External forcing can reproduce this positive PDV-like pattern (Figure 4b); thus, it dominates the positive trend of PDV index in the observation. The result is robust in all the eight models (Figure S3). However, under GHG forcing, both the eastern tropical Pacific and the North Pacific show substantial warming, with a similar magnitude (Figure 4c), consistent with the weak positive trend in PDV index (Figure 3c). The stronger warming along the equator under GHG forcing occurs in most models (Figure S4), consistent with many studies that described it as "equatorial warming" [*Liu et al.*, 2005; *DiNezio et al.*, 2009; *Xie et al.*, 2010]. Under AA forcing, the eastern tropical Pacific shows a weaker cooling than the North Pacific (Figure 4d), consistent in most of the models (Figure S5). Thus, the AA forcing favors the positive trend of PDV index (Figure 3c). When examining the combined effects of GHG and AA forcings, the strong cooling in the North Pacific under AA forcing offsets the substantial warming under GHG forcing, so the strong warming in the tropical Pacific stands out (Figure 4e). Finally, the combined effects of GHG and AA induce a stronger warming along the equator than in the North Pacific, which favors the positive phase of PDV. The SST trends pattern shows a positive PDV-like pattern under GHG and AA forcings, having a centered pattern correlation coefficient of 0.89 with that in external forcing, statistically significant at the 5% level. It indicates that the GHG and AA forcings together lead to the positive trend of PDV index in observation. The effect of natural forcing is the weakest (Figure 4f).

How are such SST trend patterns formed under GHG and AA forcing? We investigate the mechanism by heat budget analysis (Figure S6). On interdecadal and longer time scales, we can infer the total ocean heat transport effect from the net surface heat flux [*Xie et al.*, 2010]. Comparing the contributions of each heat flux based on MME, changes of the surface net longwave (shortwave) radiation favors the positive trend of PDV index under GHG (AA) forcing, which is attributed to surface downward longwave (shortwave) radiation

(Figure 5a). The increased GHGs induce an increase in downward longwave radiation, especially in the tropical Pacific (Figure 5b), leading to substantial warming in the tropics. The AA forcing reduces the surface downward shortwave radiation and cools the ocean, especially in the North Pacific (Figure 5c), inducing the positive PDV-like pattern of SST trends. Compared with the changes under clear sky, the maximum of the increase in surface downward longwave radiation over the tropical Pacific under GHG forcing still exists, indicating the weak effect of cloud there (Figures S7a and S7b). The results under GHG forcing are further confirmed by the abrupt fourfold CO_2 increase simulations (Figure S8). However, the strong reduction of surface downward shortwave radiation over the North Pacific under AA forcing weakens strongly under clear sky (Figure S7c), where the total could fraction increases significantly (Figure S7d), suggesting the importance of cloud-aerosol interaction under these conditions.

4. Summary and Discussions

The contributions of internal variability, GHGs, and AAs in regulating PDV during the twentieth century are examined by analyzing 129 realizations from eight CMIP5 models. The results show that PDV phase transition is not only dominated by internal variability but also significantly affected by external forcing. External forcing has a contribution of the negative (positive) phase during the early (late) half of twentieth century, dominating the positive trend in PDV index. A comparison of separate forcing runs shows that the combined effects of GHGs and AAs favor the positive trend of PDV index during 1861–2005. GHG forcing induces the increased surface downward longwave radiation, especially over the tropical Pacific, resulting in stronger warming there. The AA forcing induces a stronger cooling in the North Pacific region, due to the reduced surface downward shortwave radiation via cloud-aerosol interaction, which offsets the substantial warming caused by GHG forcing. Therefore, the strong warming in the tropical Pacific stands out under GHG and AA forcings, leading to a positive PDV-like pattern and the positive PDV trend in observation.

The relative roles of internal variability and external forcing in climate variability and change are currently unknown. Reductions in AAs have contributed to an intensification of precipitation in the past two decades [*Wu et al*., 2013]. The observed negative phase of PDV has contributed to the early 2000s global warming hiatus [*Meehl et al*., 2014]. Thus, to clarify the effects of different forcings in regulating PDV is important for understanding and predicting climate changes. We note a positive trend in PDV index under external forcing, which may support decadal prediction of the climate evolution over the next several decades.

Acknowledgments
This work is supported by National Natural Science Foundation of China under grant numbers 41125017 and 41330423.

The Editor thanks two anonymous reviewers for their assistance in evaluating this paper.

References

Allen, R., J. Norris, and M. Kovilakam (2014), Influence of anthropogenic aerosols and the Pacific Decadal Oscillation on tropical belt width, *Nat. Geosci.*, *7*(4), 270–274.

Arblaster, J., G. Meehl, and A. Moore (2002), Interdecadal modulation of Australian rainfall, *Clim. Dyn.*, *18*, 519–531.

Barlow, M., S. Nigam, and E. Berbery (2001), ENSO, Pacific decadal variability, and U.S. summertime precipitation, drought, and stream flow, *J. Clim.*, *14*, 2105–2128.

Bonfils, C., and D. Benjamin (2011), Investigating the possibility of a human component in various Pacific Decadal Oscillation indices, *Clim. Dyn.*, *37*(7–8), 457–1468.

Cai, W., A. Santoso, G. Wang, E. Weller, L. Wu, K. Ashok, Y. Masumoto, and T. Yamagata (2014), Increased frequency of extreme Indian Ocean Dipole events due to greenhouse warming, *Nature*, *510*(7504), 254–258.

Chen, J., A. Del Genio, B. Carlson, and M. Bosilovich (2008), The spatiotemporal structure of twentieth-century climate variations in observations and reanalyses. Part II: Pacific pan-decadal variability, *J. Clim.*, *21*, 2634–2650.

Deser, C., A. Phillips, and J. Hurrell (2004), Pacific interdecadal climate variability: Linkages between the tropics and the North Pacific during boreal winter since 1900, *J. Clim.*, *17*, 3109–3124.

Deser, C., A. Phillips, and M. Alexander (2010), Twentieth century tropical sea surface temperature trends revisited, *Geophys. Res. Lett.*, *37*, L10701, doi:10.1029/2010GL043321.

DiNezio, P., A. Clement, G. Vecchi, B. Soden, B. Kirtman, and S. Lee (2009), Climate response of the equatorial Pacific to global warming, *J. Clim.*, *22*, 4873–4892.

Fang, C., L. Wu, and X. Zhang (2014), The impact of global warming on the Pacific Decadal Oscillation and the possible mechanism, *Adv. Atmos. Sci.*, *31*(1), 118–130.

Fedorov, A., and S. Philander (2000), Is El Niño changing?, *Science*, *288*, 1997–2002.

Furtado, J., E. Lorenzo, N. Schneider, and N. Bond (2011), North Pacific decadal variability and climate change in the IPCC AR4 models, *J. Clim.*, *24*, 3049–3066.

IPCC: Climate Change (2013), *The Physical Science Basis. Contribution of Working Group 1 to the Fifth Assessment Report of the Intergovernmental Panel on Climate Change*, edited by T. F. Stocker et al., Cambridge Univ. Press, Cambridge, U. K., and New York, doi:10.1017/CBO9781107415324.004.

Jha, B., Z. Hu, and A. Kumar (2014), SST and ENSO variability and change simulated in historical experiments of CMIP5 models, *Clim. Dyn.*, *42*, 2113–2124.

Lapp, S., J. St. Jacques, E. Barrow, and D. Sauchyn (2011), GCM projections for the Pacific Decadal Oscillation under greenhouse forcing for the early 21st century, *Int. J. Climatol.*, *31*, 1423–1442, doi:10.1002/joc.2364.

Li, H., A. Dai, T. Zhou, and J. Lu (2010), Responses of East Asian summer monsoon to historical SST and atmospheric forcing during 1950–2000, *Clim. Dyn.*, *34*, 501–514.
Liu, Z., S. Vavrus, F. He, N. Wen, and Y. Zhong (2005), Rethinking tropical ocean response to global warming: The enhanced equatorial warming, *J. Clim.*, *18*, 4684–4700.
Mantua, N., and S. Hare (2002), The Pacific Decadal Oscillation, *J. Oceanogr.*, *58*, 35–44.
Mantua, N., S. Hare, Y. Zhang, J. Wallace, and R. Francis (1997), A Pacific interdecadal oscillation with impacts on salmon production, *Bull. Am. Meteorol. Soc.*, *78*, 1069–1079.
Meehl, G., A. Hu, and B. Santer (2009), The mid-1970s climate shift in the Pacific and the relative roles of forced versus inherent decadal variability, *J. Clim.*, *22*, 780–792.
Meehl, G., H. Teng, and J. Arblaster (2014), Climate model simulations of the observed early-2000s hiatus of global warming, *Nat. Clim. Change*, doi:10.1038/nclimate2357.
Power, S., T. Casey, C. Folland, A. Colman, and V. Mehta (1999), Interdecadal modulation of the impact of ENSO on Australia, *Clim. Dyn.*, *15*, 319–324.
Qian, C., and T. Zhou (2014), Multidecadal variability of North China aridity and its relationship to PDO during 1900–2010, *J. Clim.*, *27*(3), 1210–1222.
Smith, T., R. W. Reynolds, T. C. Peterson, and J. Lawrimore (2008), Improvements to NOAA's historical merged land-ocean surface temperature analysis (1880–2006), *J. Clim.*, *21*, 228–2296.
Taylor, K., R. Stouffer, and G. Meehl (2012), An overview of CMIP5 and the experiment design, *Bull. Am. Meteorol. Soc.*, *93*, 485–498.
Verdon, D., and S. Franks (2006), Long-term behaviour of ENSO: Interactions with the PDO over the past 400 years inferred from paleoclimate records, *Geophys. Res. Lett.*, *33*, L06712, doi:10.1029/2005GL025052.
Wang, H. (2002), The instability of the East Asian summer monsoon–ENSO relations, *Adv. Atmos. Sci.*, *19*, 1–11.
Wang, T., O. Otterå, Y. Gao, and H. Wang (2012), The response of the North Pacific decadal variability to strong tropical volcanic eruptions, *Clim. Dyn.*, *39*(12), 2917–2936.
Wu, P., N. Christidis, and P. Stott (2013), Anthropogenic impact on Earth's hydrological cycle, *Nat. Clim. Change*, *3*(9), 807–810.
Xiang, B., B. Wang, and T. Li (2013), A new paradigm for the predominance of standing central Pacific warming after the late 1990s, *Clim. Dyn.*, *41*(2), 327–340.
Xie, S., C. Deser, G. A. Vecchi, J. Ma, H. Teng, and A. T. Wittenberg (2010), Global warming pattern formation: Sea surface temperature and rainfall, *J. Clim.*, *23*, 966–986.
Xie, S., B. Lu, and B. Xiang (2013), Similar spatial patterns of climate responses to aerosol and greenhouse gas changes, *Nat. Geosci.*, *6*, 828–832.
Yeh, S., Y. Ham, and J. Lee (2012), Changes in the tropical Pacific SST trend from CMIP3 to CMIP5 and its implication of ENSO*, *J. Clim.*, *25*, 7764–7771.
Yoon, J., and S. Yeh (2010), Influence of the Pacific Decadal Oscillation on the relationship between El Niño and the northeast Asian summer monsoon, *J. Clim.*, *23*, 4525–4537.
Yu, L., T. Furevik, O. Otterå, and Y. Gao (2014), Modulation of the Pacific Decadal Oscillation on the summer precipitation over East China: A comparison of observations to 600-years control run of Bergen Climate Model, *Clim. Dyn.*, doi:10.1007/s00382-014-2141-5.
Zheng, X., S. Xie, Y. Du, L. Liu, G. Huang, and Q. Liu (2013), Indian Ocean dipole response to global warming in the CMIP5 multimodel ensemble, *J. Clim.*, *26*, 6067–6080.
Zhou, T., and R. Yu (2006), Twentieth century surface air temperature over China and the globe simulated by coupled climate models, *J. Clim.*, *19*(22), 5843–5858.
Zhou, T., D. Gong, J. Li, and B. Li (2009), Detecting and understanding the multi-decadal variability of the East Asian summer monsoon—Recent progress and state of affairs, *Meteorol. Z.*, *18*(4), 455–467.
Zhou, T., F. Song, R. Lin, X. Chen, and X. Chen (2013), The 2012 North China floods: Explaining an extreme rainfall event in the context of a long-term drying tendency [in "Explaining Extreme Events of 2012 from a Climate Perspective"], *Bull. Am. Meteorol. Soc.*, *94*(9), S49–S51.